Measurement of neutron-induced fission cross sections of ^{235}U and ^{238}U relative to n-p scattering at CSNS Back-n facility

Yonghao Chen[1, 2*], Yiwei Yang[3], *Zhizhou* Ren[3, 4], *Wei* Jiang[1, 2], *Ruirui* Fan[1, 2], *Han* Yi[1, 2], *Rong* Liu[3], *Jingyu* Tang[1, 2], *Hantao* Jing[1, 2], *Yang* Li[1, 2], *Qiang* Li[1, 2], *Zhixin* Tan[1, 2] (CSNS Back-n collaboration)

[1]Institute of High Energy Physics, Chinese Academy of Sciences (CAS), 100049 Beijing, China
[2]Spallation Neutron Source Science Center, 523803 Dongguan, China
[3]Institute of Nuclear Physics and Chemistry, China Academy of Engineering Physics, 621900 Mianyang, China
[4]Department of Modern Physics, University of Science and Technology of China, 230026 Hefei, China

Abstract. ^{235}U and ^{238}U are very important isotopes in the nuclear energy system. Their neutron-induced fission cross sections have been measured intensively and evaluated as standard up to 200 MeV. However, as a matter of fact, the experimental data in the high-energy region are scarce. This work reports the measurement of $^{235, 238}$U(n, f) cross sections relative to n-p scattering performed at the China Spallation Neutron Source (CSNS) back-streaming neutron facility (Back-n). Preliminary results of $^{235, 238}$U(n, f) cross sections from 10 to 66 MeV are obtained, which are generally following the shape of the IAEA standard. However, significant discrepancies are observed at some given energies, which will be further studied.

1 Introduction

^{235}U and ^{238}U are very important isotopes in the nuclear energy system, since ^{235}U is the fissile material in the current thermal reactor, and ^{238}U is the fertile material in the future U-Pu cycle. Neutron-induced fission cross sections of ^{235}U and ^{238}U have been extensively measured in past several decades and evaluated as standard in a wide neutron energy range [1]. Therefore $^{235, 238}$U(n, f) cross-section data are always used as references, such as for the fission cross-section measurement and the neutron flux determination. In those cases of using them as references, the accuracy of $^{235, 238}$U(n, f) cross section is of great importance since any error will be propagated to subsequent analysis. However, the experimental data in the high-energy region, especially above 30 MeV, are scarce. There are so far only several measurements [2-10] above 30 MeV, and the discrepancies among different measurements are significant for both of ^{235}U and ^{238}U. It is consequently indispensable to measure the fission cross sections of ^{235}U and ^{238}U in the high-energy region, which will be contributing to the nuclear data evaluation.

In this paper, we will present the measurement of $^{235, 238}$U(n, f) cross sections performed at back-streaming neutron beam (Back-n) at the China Spallation Neutron Source (CSNS). The facility and detectors will be briefly introduced in sec. 2. The data analysis and preliminary results will be shown in sec. 3. Section 4 will draw conclusions and point out the following work.

2 Facility and experimental setup

2.1 CSNS Back-n beam line

CSNS is a multidisciplinary research platform started commissioning since 2018. Spallation neutrons are generated by bombarding 1.6 GeV protons to a thick tungsten target with a 25-Hz repetition frequency. CSNS is mainly used for material study based on the neutron scattering technique but expanded applications, such as proton beam, muon beam and white neutron beam, are involved as well.

Back-n beam line is built as a reserve extension of the incident proton beam line, which is exploiting the back-streaming neutrons for use. Thanks to its unique design, Back-n is characterized by a wide energy range (0.5 eV–300 MeV) and weak γ-flash compared to forward direction. More details of the Back-n facility and its activities might be found in Ref. [11-14].

2.2 Experimental setup

The detectors were installed at Back-n end station 1 (ES#1), which was about 57 meters away from the spallation target. A fission ionization chamber for the cross-section measurement (FIXM) [15] was upstream placed as shown in fig. 1. Two ^{235}U and two ^{238}U samples were mounted in the chamber. All the samples inside FIXM are circular in diameters of 50 mm with masses of a few milligrams.

* Corresponding author: chenyonghao@ihep.ac.cn

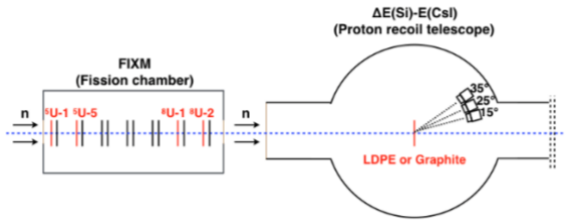

Fig. 1. Experimental setup at Back-n ES#1.

Proton recoil telescopes (PRTs) were downstream installed in a chamber after FIXM for measuring the n-p scattering. The chamber was maintained at 5×10^{-3} Pa during the measurement. It provided a well-defined geometry relation between the beam, detectors and sample. The PRT consisted of a silicon detector (Si-PIN) and a thallium activated cesium iodide scintillator (CsI(Tl)). A low-density polythene (LDPE) sample was placed in the chamber center and three PRTs were located, respectively, at 15°, 25° and 35° relative to the beam axis. Only PRT at 25° were used in this work whose distance to sample center was 240 mm. A graphite sample with an equivalent thickness was measured as well to determine the background protons generated via the ^{12}C(n, p) reaction. The diameter of the neutron beam spot in this measurement was about φ18 mm. The beam was fully covered by all the samples.

3 Data analysis and preliminary results

The fission cross section σ_f at neutron energy E_n can be calculated by

$$\sigma_f(E_n) = \frac{R_f(E_n)}{R_{np}(E_n)} \times \frac{N_H}{N_U} \times \frac{\varepsilon_{np}(E_n)}{\varepsilon_f(E_n)} \times \sigma_{np}(E_n), \quad (1)$$

where the subscripts *f* and *np* stand for fission and n-p scattering, R is the reaction rate, N_H and N_U are the areal density of the hydrogen and uranium atoms, ε is the detection efficiency, σ_{np} is the n-p scattering cross section.

3.1 Analysis of FIXM

3.1.1 Neutron time-of-flight (TOF) method

The TOF technique is used to determine the incident neutron energy according to

$$v = \frac{L}{T-T_0}, \quad (2)$$

$$T_0 = T_g - \frac{L}{c}, \quad (3)$$

where v is the neutron velocity, L is the length of the flight path, T is the timing that neutrons arrive the sample, T_0 is the starting time of the neutron flight. T_0 is calibrated by the γ-ray events as shown in eq. (3), where T_g is the timing of the γ-induced fission events and c is the speed of the light. Flight path L is calibrated by the resonances of ^{235}U(n, f). More details of the TOF method of the fission chamber at Back-n may be found in Ref. [14].

The neutron TOF can be obtained once the L and T_0 are defined. Figure 2 shows the two-dimensional (2D) distribution of TOF versus the signal amplitude of ^{235}U-1 and ^{238}U-1 sample. Fission events with large amplitudes can be clearly discriminated against the low-amplitude events, which are mainly from the α decay of the samples and the (n, lcp) reactions.

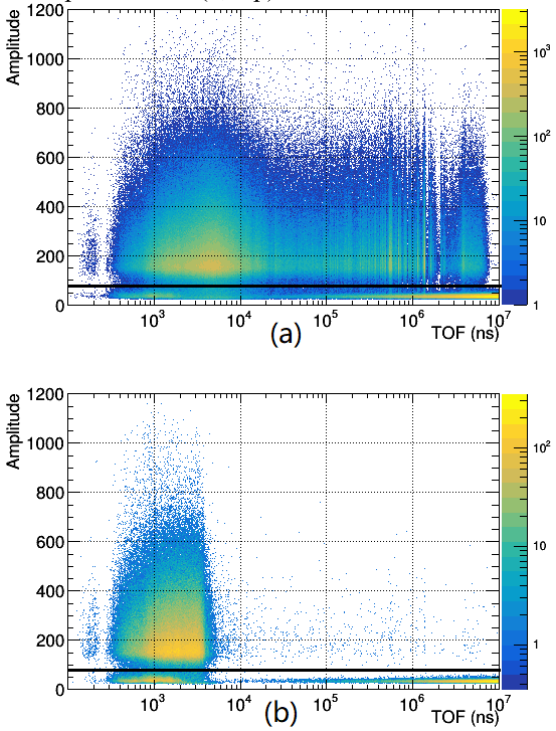

Fig. 2 2D distribution of neutron TOF versus the amplitude of ^{235}U-1 (a) and ^{238}U-1 (b).

3.1.2 Double-bunch unfolding

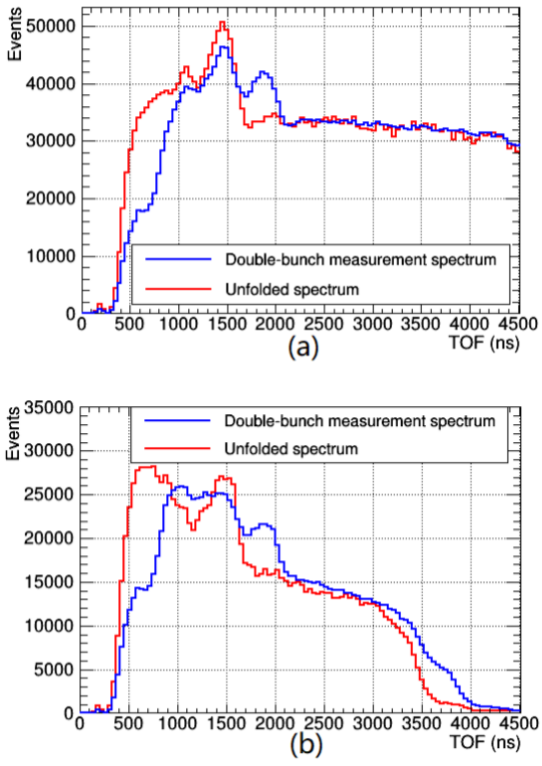

Fig. 3 TOF spectrum of double-bunch measurement (blue) and its unfolded results (red) of ^{235}U (a) and ^{238}U (b).

The blue curves in fig. 3 are the fission rates of ^{235}U and ^{238}U as a function of neutron TOF measured in

double-bunch mode. Double-bunch is the general operation mode of CSNS accelerator, which means there are two identical proton bunches with a fixed interval (410 ns) in each proton pulse. Care must be taken because it is affecting the accuracy of the TOF calibration, especially for high-energy neutrons whose TOF are short. Due to the nature of the double-bunch mode, the measured TOF spectrum can be considered as an overlap of two identical single-bunch TOF spectrum with a delay of 410 ns. An iterative algorithm based on Bayes' theorem was developed for unfolding Back-n double-bunch TOF spectrum, which is described in details in a dedicated paper [16]. The unfolded TOF spectra of ^{235}U and ^{238}U are shown as the red curves in fig. 3. The fission rate as a function of neutron energy is then obtained by resampling the unfolded TOF spectrum and converting the TOF to energy.

3.2 Analysis of PRT

3.2.1 Neutron TOF method

The TOF calibration of PRT is similar to the case of FIXM. Since n-p scattering is not showing any resonance, a tantalum sample is used for calibrating the flight length based on the strong resonances of ^{181}Ta(n, γ) at eV region. The γ-flash signal of Si detector is used to define the T_0. It should be mentioned that the unfolding method described in 3.1.2 is used as well to unfold the neutron TOF spectrum measured by PRT.

3.2.2 Particle identification (PID)

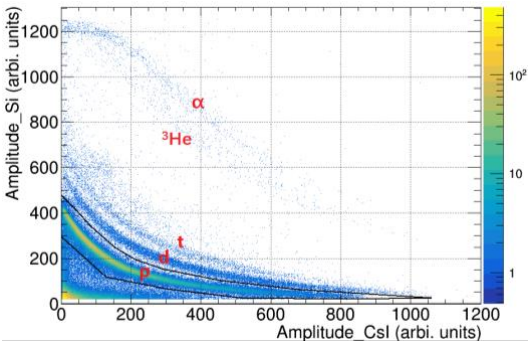

Fig. 4 ΔE-E distribution of LDPE sample.

The PRT uses the Δ*E*-*E* method for PID. The thin Si detector is used for measuring the partial energy (Δ*E*) of crossed particles. The thick CsI (Tl) scintillator fully stops the charged particles and measures the remaining energy *E*. Figure 4 presents the ΔE-E distribution of LDPE sample. Different particles are clearly distinguished from each other, and protons are selected by a graphical cut.

3.2.3 N-p elastic scattering rate

A graphite sample with equivalent thickness is measured to subtract the background protons generated via the ^{12}C(n, p) reactions in the LDPE sample. The measurement and analysis for graphite sample are exactly same as for the LDPE sample. Figure 5 shows the proton event distribution as a function of neutron energy of LDPE and graphite samples. The black one is the n-p elastic scattering rate obtained by subtracting the graphite contribution from the measurement of the LDPE sample.

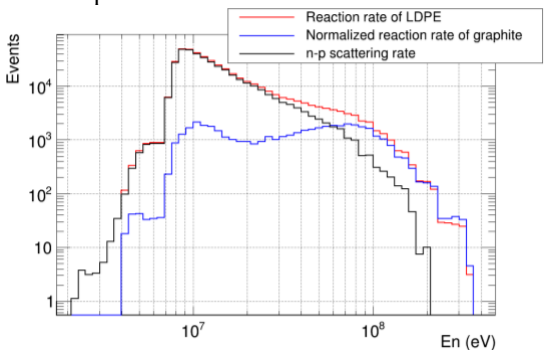

Fig. 5 Proton events distribution as a function of neutron energy.

3.2.4 Efficiency Simulation

The efficiency of the PRT is studied by the Geant4 [17-18] simulation. The detector system is reproduced in the simulation. The evaluated data library ENDF/B-VIII.0 is used to replace the default G4NDL neutron data [19-21]. The actual Back-n energy spectrum from 10 to 100 MeV is used as the primary neutron beam in the simulation. A LDPE and a graphite sample having the same thicknesses as the experimental ones are, respectively, simulated. The simulated n-p scattering rate is obtained by subtracting the contribution of the graphite sample. Three different physics lists (*BERT, BIC and INCLXX*) are compared and *BERT* (with High Precision model) is finally used since it best matches the experiment data with deviations less than 5% in the range of 10-70 MeV. The fraction of the scattering protons detected by PRT over all the n-p scattering events in the LDPE sample is defined as effective efficiency, which is shown in fig. 6.

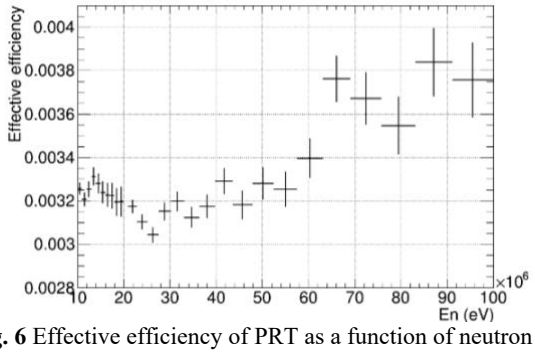

Fig. 6 Effective efficiency of PRT as a function of neutron energy.

3.3 Preliminary results

Since the sample homogeneity and beam profile are not well known in this work, it is difficult to extract the absolute neutron flux and determine the cross sections absolutely. Instead, we are doing a shape measurement and normalizing the $^{235, 238}$U(n, f) cross sections to the IAEA standards [1] at 14.5 MeV. The n-p scattering cross sections are taken from IAEA standards [1] and JEFF-3.1.2 [22], respectively, for neutrons below and

above 20 MeV. The efficiency of the fission chamber (FIXM) is supposed to be constant, therefore it is not needed for a shape measurement.

Figures 7 and 8 show the preliminary results of ^{235,238}U(n, f) cross sections from 10 to 66 MeV together with other measurements [4-6, 8-10, 23-25]. The statistical errors of this work are ranging from less than 1% up to 6%. It can be observed that the measured shape in this work generally follows the IAEA standards, but significant discrepancies exist at some given energies.

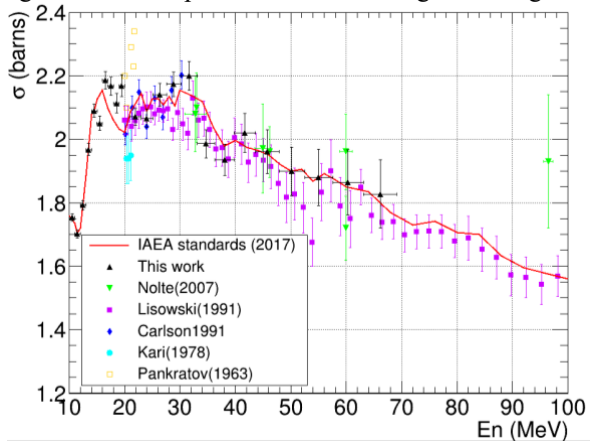

Fig. 7 ^{235}U(n, f) cross sections measured in this work in comparison with other measurements [4-6, 23-24] (only statistical errors are included for this work).

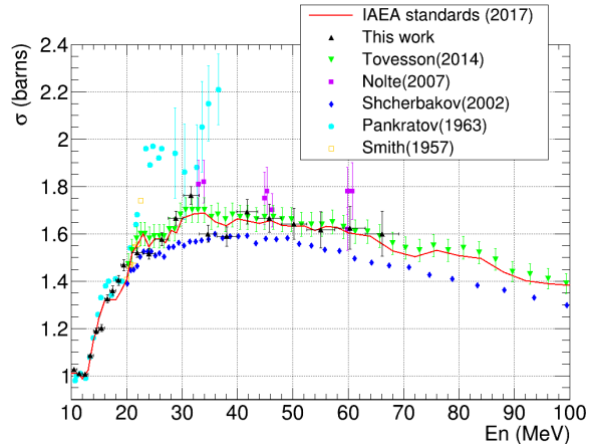

Fig. 8 ^{238}U(n, f) cross sections measured in this work in comparison with other measurements [5-6, 8-9, 25] (only statistical errors are included for this work).

4 Conclusions and future work

This work reports preliminary results of the $^{235, 238}$U(n, f) cross-section measurement from 10 to 66 MeV, which is performed at the CSNS Back-n beam line. The measured shapes generally follow the IAEA standards within statistical errors. However, significant deviations are observed at some given energies.

In this work, we used Geant4 to simulate the effective efficiency, as defined in sec. 3.2.4, and extract the neutron flux based on the n-p scattering cross sections. In fact, we can just simulate the solid angle of PRT and use the differential n-p scattering cross sections to obtain the neutron flux as well. This is supposed to be more straightforward and is foreseen to be done in the near future. Besides, this work is a shape measurement instead of absolute measurement. An absolute measurement will be possible when we have a good knowledge of sample homogeneity and beam profile.

This research was supported by Guangdong Basic and Applied Basic Research Foundation (Grant Nos. 2020A1515010360 and 2022B1515120032), the National Natural Science Foundation of China (Grant No. 11905031), Youth Innovation Promotion Association CAS, Xie Jialin Foundation of Institute of High Energy Physics (Grant No. E15467U2).

References

1. A. D. Carlson et al., Nucl. Data Sheets **148**, 143 (2018)
2. V. I. Goldanskii et al, J. Exp. Theoretical Phys. **2**, 677 (1956)
3. J. Rapaport et al., Los Alamos Scientific Lab. Reports No. 11078-MS, p.1 (1987)
4. P. W. Lisowski et al., Nucl. En. Agency Nucl. Data Committee reports No. 305, p. 177 (1991)
5. R. Nolte et al., Nucl. Sci. Eng. **156**, 197 (2007)
6. V. M. Pankratov et al., Atomnaya Energiya **14**, 177 (1963)
7. V. P. Eismont et al., Phys. Rev. C **53**, 2911 (1996)
8. O. Shcherbakov et al., J. Nucl. Sci. Technol. Suppl. **2**, 230 (2002)
9. F. Tovesson et al., Nucl. Sci. Eng. **178**, 57 (2014)
10. Z. W. Miller, Ph. D thesis submitted to University of Kentucky (2015)
11. J. Y. Tang et al., Nucl. Sci. Tech. **32**, 11 (2021)
12. J. Y. Tang et al., Chin. Phys. C **45**, 062001 (2021)
13. H. T. Jing et al., Nucl. Instrum. Methods A **621**, 91 (2010)
14. Y. H. Chen et al., Eur. Phys. J. A **55**, 155 (2019)
15. Y. W. Yang et al., Nucl. Instrum. Methods A **940**, 486 (2019)
16. H. Yi et al., J. Instrum. **15**, 03026 (2020)
17. S. Agostinelli et al., Nucl. Instrum. Methods A **506**, 250 (2003)
18. J. Allison et al., IEEE Trans. Nucl. Sci. **53**, 270 (2006)
19. E. Mendoza et al., IEEE Trans. Nucl. Sci. **61**, 2357 (2014)
20. E. Mendoza et al., IAEA technical report INDC(NDS)-0612, Vienna (2012)
21. E. Mendoza et al., IAEA technical report INDC(NDS)-0758, Vienna (2018)
22. https://www.oecd-nea.org/dbdata/jeff/
23. K. Kari, Kernforschungszentrum Karlsruhe Reports, No. 2673 (1978)
24. A. D. Carlson et al., Conf. on Nucl. Data for Sci. and Technol., Juelich 1991, p. 518 (1991)
25. R. K. Smith et al., Bull. Am. Phys. Soc. Ser. II **2**, 196 (1957)